Electromagnetic Wave Scattering From a Forest or Vegetation Canopy: Ongoing Research at the University of Texas at Arlington

Mostafa A. Karam[1], *Faouzi Amar, and Adrian K. Fung*
Wave Scattering Research Center
Department of Electrical Engineering
UTA Box 19016
University of Texas at Arlington
Arlington, Texas 76019, USA

[1]NASA Goddard Space Flight Center
Mail Code 975
Greenbelt, Maryland 20771, USA

Abstract

The Wave Scattering Research Center (WSRC), at the University of Texas at Arlington (UTA), has developed a scattering model for forest or vegetation, based on the theory of electromagnetic-wave scattering in random media. The model generalizes the assumptions imposed by earlier models, and compares well with measurements from several forest canopies.

This paper gives a description of the model. It also indicates how the model elements are integrated to obtain the scattering characteristics of different forest canopies. The scattering characteristics may be displayed in the form of polarimetric signatures, represented by like- and cross-polarized scattering coefficients, for an elliptically-polarized wave, or in the form of signal-distribution curves. Results illustrating both types of scattering characteristics are given.

1. Introduction

Electromagnetic-wave scattering from forest and vegetation canopies has been the subject of intensive studies by numerous scientific communities, such as remote sensing and communications. The remote-sensing community is interested in relating the field scattered from a forest or vegetation canopy to its geometric and biophysical characteristics. The communications community is interested in studying the radio-link performance, and how it is affected by wave attenuation, fading, and co-channel interference, due to the presence of a forest canopy somewhere along the path of the link.

The Wave Scattering Research Center (WSRC) at the University of Texas at Arlington (UTA) has been involved in the studies of electromagnetic-wave scattering and propagation in forest and vegetation for a long time. Recently, the center has developed a scattering model for forest and vegetation canopies [1] which generalizes several assumptions imposed by earlier models for closed canopies [2-12].

All existing models can be grouped into two categories, either phenomenological or physical. The phenomenological models [2, 3] are based on the intuitive understanding of the relative importance of different forest components, such as branches, twigs, trunks, leaves, soil, and understory cover. The scattering model is then constructed by summing up the contributions, from each forest component believed to be important. The individual scattering mechanisms are modeled using empirical or analytical descriptions, as appropriate. Despite the encouraging results obtained through phenomenological models, their domain of applicability is limited due to several reasons:

(i) each model is valid only for a certain type of vegetation canopy or a certain tree stand, under specific environmental conditions,

(ii) each model can be used only for a certain frequency band,

(iii) the vegetation parameters have not been fully accounted for within such models, and

(iv) the electromagnetic interaction with forest components is not well represented.

The physical models are based on the interaction of electromagnetic waves with forest or vegetation canopies [1, 4-12]. A canopy can be modeled either as a discrete [1, 4-11] or a continuous random medium [12]. The radiative transfer theory [4-10], or the distorted Born approximation [11], have been applied to study electromagnetic interactions with such random media. Most of the existing physical models are restricted, by assumptions with respect to the shape of the scatterers [9], or by the applicable frequency range [2, 10]. Some models account only for leaves [7] and not branches, while others treat branches and soil surface but not leaves [8].

Recently, the Michigan Microwave Canopy Scattering model (MIMICS) was proposed [4], and used to model multi-angle and temporal backscatter from a walnut orchard [5, 6]. MIMICS is based on the first-order solution of the radiative transfer theory, and involves the following assumptions:

(i) The contribution from trunks in the backscattering direction can be ignored.

(ii) The cross polarized term in the trunk phase matrix is ignored.

(iii) In the canopy-ground interaction, the ground is modeled as a flat surface.

(iv) The optical (forward scattering) theorem [13-15] can be used to calculate the extinction coefficient within the canopy. The theorem is accurate to the extent that the amplitude of the scattered field is accurate. Under a low-frequency approxima-

tion, this theorem can only provide the loss due to absorption. Hence, scattering losses are not included [15].

(v) Either the Physical Optics or Rayleigh approaches can be used to calculate scattering from leaves. The Physical Optics approach is applicable to leaves larger than the operational wavelength, and the Rayleigh approach is applicable to very small leaves. Thus, MIMICS can not accommodate leaves with intermediate sizes.

(vi) Only single scattering is considered. This may be true for lower frequencies and for sparse vegetation. However, for higher frequencies or for dense canopies, multiple-scattering effects may become very important. This is one of the reasons why MIMICS predictions are lower at X-band than measured values [6].

In view of the above, the scattering model developed at WSRC is aimed at generalizing the assumptions by:

(i) including surface-roughness effects from soil and canopy-soil interaction;

(ii) accounting for various branch sizes and their orientation distribution;

(iii) accounting for cross-polarized scattering due to trunk-ground interaction, and double-bounce volume scattering;

(iv) using an extinction formulation which accounts for both ohmic and scattering losses, when low frequency approximations are made; and

(v) including the second-order radiative-transfer solution to account for multiple scattering within the canopy.

This model has been proven to work over a wide frequency range in the microwave region. It is currently in use by several remote-sensing centers, among which are the Centre d'Etude Spatiale de Rayonnements of France, the Joint Research Council of Italy, and the Agricultural University of Wagening of The Netherlands. It is used in conjunction with synthetic-aperture radar (SAR) images, for extracting forest and vegetation parameters.

2. The modeling approach

The basic approach taken by the WSRC in developing this model is three-fold. First, a scattering model is derived for each forest component, such as a leaf (elliptical disk), a branch, or a trunk (a dielectric cylinder), and for the rough-soil surface. Second, the forest-canopy model is developed in terms of the above components, by adding the direct contribution, as well as contributions due to interactions between the various components. Third, the model is verified by testing it against measurements from different canopy sites and types.

2.1. Geometry and biophysical properties of forest components

Any forest or vegetation canopy is composed of different components, such as leaves, stems, branches, trunks, and soil. Each component has its own geometric and biophysical characteristics. The geometric characteristics (such as shape, dimension, orientation, and number density) determine the level of the scattered signal along a given direction, for a set of radar parameters (i.e., angle, frequency, and polarization). The biophysical characteristics (such as water content and water potential) have a strong influence on the dielectric constant of the components.

To account for the geometric effects of the forest components, we modeled them using scatterers with the same general shape, dimensions, and orientation distributions. For example, a branch or a trunk scatterer was modeled by a finite dielectric circular cylinder. A stem or a coniferous leaf was modeled by a needle. A deciduous leaf was modeled by an elliptic or circular disc. The soil-canopy interface was modeled by an irregular random surface.

To account for the biophysical effects, we used an empirical formulation to estimate the dielectric constant of a leaf [16]. The empirical model takes into account the gravitational water content, the bulk density, the temperature of the leaf, and is a function of frequency. Similarly, we used another empirical model to determine the dielectric constant of a soil surface [17]. This model accounts for the soil texture, the volumetric water content, and the incident frequency. On the other hand, no dielectric constant formula for the tree branches has been reported in the literature. Hence, measured values for the branch dielectric constants have been used.

2.2. Electromagnetic wave scattering by forest components

The electromagnetic-wave interaction with a forest component is represented by the scattering-amplitude tensor (the S matrix), which can be used to calculate its extinction and scattering properties. More specifically, the extinction coefficients can be obtained from the scattering-amplitude tensor by applying the forward-scattering theorem (the optical theorem) [13-15]. The Müeller matrix, which describes the scattering properties, can be found from the coherency product of the scattering-amplitude tensor [15]. Based on the Helmholtz integral [18], the scattering-amplitude tensor is $\overline{\overline{\mathbf{F}}}(\hat{\mathbf{s}},\hat{\mathbf{i}})$. For a forest component illuminated by a plane wave propagating in the $\hat{\mathbf{i}}$ direction, with an electric field given by

$$\overline{\mathbf{E}}_0(\bar{r}) = \sum_{q=v,h} \hat{\mathbf{q}}_i\, \hat{\mathbf{q}}_i \cdot \overline{\mathbf{E}}_0\, e^{-jk\hat{\mathbf{i}}\cdot\bar{r}} = \left(\overline{\overline{\mathbf{I}}} - \hat{\mathbf{i}}\hat{\mathbf{i}}\right)\cdot \overline{\mathbf{E}}_0\, e^{-jk\hat{\mathbf{i}}\cdot\bar{r}}, \qquad (1)$$

this can be rewritten as [7-8]

$$\overline{\overline{\mathbf{F}}}(\hat{\mathbf{s}},\hat{\mathbf{i}})\cdot\overline{\mathbf{E}}_0 = \frac{k}{4\pi}\left(\overline{\overline{\mathbf{I}}} - \hat{\mathbf{i}}\hat{\mathbf{i}}\right)\cdot\int d\bar{r}'(\varepsilon_r - 1)\overline{\mathbf{E}}_i(r')e^{jk\hat{\mathbf{s}}\cdot\bar{r}'}, \qquad (2)$$

where $\overline{\mathbf{E}}_0$ is the amplitude of the incident field, $\hat{\mathbf{q}}_i$ ($= v, h$) is the incident-field polarization vector, $\hat{\mathbf{s}}$ is the unit vector along the observation direction (see Figure 1), $\overline{\overline{\mathbf{I}}}$ is the unit dyad, k is the wave number of the background medium (free space), ε_r is the relative dielectric constant of the forest component, and $\overline{\mathbf{E}}_i(r')$ is the field inside the forest component.

In Equation (2), the main task in the scattering-amplitude tensor calculation is to estimate the inner field. Since the Rayleigh estimation for the inner field is valid only for very small scatterers [8-9], and the Rayleigh-Gans approximation is valid only for a tenuous scatterer [14], the Generalized Rayleigh-Gans approximation has been applied, to estimate the inner field inside a disc- or needle-shaped leaf. For the incident plane wave in Equation (1), the Generalized Rayleigh-Gans approximation for the inner field can be written as [7, 18]

$$\overline{\mathbf{E}}_i(\bar{r}') = \overline{\overline{\alpha}}\cdot\overline{\mathbf{E}}_0(\bar{r}') = \overline{\overline{\alpha}}\cdot\left(\overline{\overline{\mathbf{I}}} - \hat{\mathbf{i}}\hat{\mathbf{i}}\right)\cdot\overline{\mathbf{E}}_0\, e^{-jk\hat{\mathbf{i}}\cdot\bar{r}'} \qquad (3)$$

$\overline{\overline{\alpha}}$ in Equation (3) is the polarizability tensor [7, 18]. This inner-field estimation can be applied only to a scatterer having at least one dimension very small compared with the incident wavelength (a

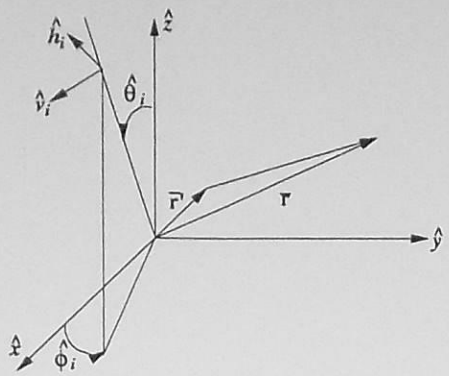

Figure 1. The polarization vectors of the incident field.

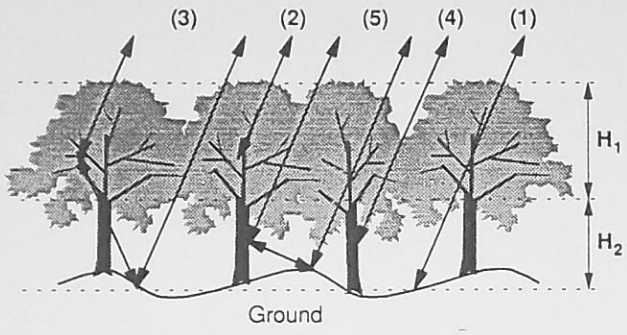

Figure 2. Geometry of a forest canopy and the backscattering processes for the zero- and first-order solutions of the radiative-transfer equation: (1) zero-order, (2) crown scattering, (3) crown-ground interaction, (4) trunk scattering, (5) trunk-ground interaction.

disc or needle). The disc radius or the needle length may be of the order of a wavelength or higher, as long as the other dimensions are very small with respect to the wavelength, which is the case for a deciduous leaf (thickness ≈ 0.2 mm) or a coniferous leaf (radius ≈ 1 cm). The Rayleigh estimate for the inner field can be obtained from Equation (3) by letting the exponential term go to unity [8-9].

By substituting Equation (3) into Equation (2), the scattering-amplitude tensor, under the Rayleigh-Gans approximation, can be written as

$$\overline{\overline{\mathbf{F}}}(\hat{\mathbf{s}},\hat{\mathbf{i}}) = \left[\frac{k^2}{4\pi} v_o (\varepsilon_r - 1)(\overline{\overline{\mathbf{I}}} - \hat{\mathbf{s}}\hat{\mathbf{s}}) \cdot \overline{\overline{\alpha}} \cdot (\overline{\overline{\mathbf{I}}} - \hat{\mathbf{i}}\hat{\mathbf{i}})\right] \mu(\hat{\mathbf{s}},\hat{\mathbf{i}}), \qquad (4)$$

where v_o is the scatterer volume, and is given by the Debye interference function

$$\mu(\hat{\mathbf{s}},\hat{\mathbf{i}}) = \frac{1}{v_o}\int d\bar{\mathbf{r}}\, e^{jk(\hat{\mathbf{s}}-\hat{\mathbf{i}})\cdot\bar{\mathbf{r}}} \qquad (5)$$

In Equation (5), the integration is performed over the volume of the forest component. Explicit expressions for the scattering-amplitude tensor of randomly-oriented elliptic discs and needles are given in [7].

Tree branches and trunks are modeled as finite cylinders. As such, the inner field can be estimated by the field inside a similar cylinder of infinite length. This estimation is valid for a branch with a length-to-diameter ratio greater than 5 [8, 18].

For the soil surface, a scattering model based on an integral-equation method (IEM) [19] is used. This model has several merits, since

(i) it accounts for both like and cross polarizations;

(ii) the like polarization contains both single-scattering and multiple-scattering terms;

(iii) for a slightly-rough surface, the like-polarized, single-scattering terms reduce to the first-order solution, derived from the small-perturbation method [19]; and

(iv) for very large surface roughness and small surface slopes, the single-scattering term agrees with the standard Kirchhoff model [20].

2.3. Geometry of a forest canopy

The geometry of a forest canopy is given in Figure 2, where the canopy is modeled as a two-layer medium above a rough interface. The upper layer represents the crown, the lower layer represents the trunk, and the rough interface represents the soil surface. The crown layer contains the branches, the leaves, and the stems. The branches may be separated into different groups, according to their sizes. Each branch group has its own orientation distribution. In a similar way, the trunk layer may also contain several groups, if needed. A generalization of the canopy model to allow multiple layers has been implemented [21]. Further generalization of the scattering model, to account for open-canopy structure and different shapes of the tree crowns, is underway.

2.4. Electromagnetic wave interaction with a forested canopy

When considering electromagnetic-wave interaction with a forest or a vegetation canopy, two approaches may be taken: the vector radiative-transfer-theory approach, or a numerical-simulation approach. The vector radiative-transfer theory is used to determine the bistatic-scattering coefficients [13] and polarimetric signatures [21]. Numerical simulation is used to calculate the probability distribution function of the amplitude and the phase of the scattered field [24]. Both approaches are discussed.

2.4.1. The vector radiative-transfer-equation approach

The vector radiative-transfer theory describes the intensity propagation (Stokes-parameter vector) within the canopy, through an integro-differential equation, given by [14, 15, 20]

$$\cos(\theta)\frac{d\bar{\mathbf{I}}(z,\theta,\phi)}{dz} = -\overline{\overline{\kappa}}(\theta,\phi)\bar{\mathbf{I}}(z,\theta,\phi) + \int_0^{2\pi} d\phi' \int_0^{\pi} d\theta' \overline{\overline{\mathbf{P}}}(\theta,\phi;\theta',\phi')\bar{\mathbf{I}}(z,\theta',\phi') \qquad (6)$$

where $\mathbf{I}(\mathbf{z},\theta,\phi)$ is the Stokes-parameter vector (intensity), propagating in the (θ,ϕ) direction, at a location defined by z, with

$$\bar{\mathbf{I}}(\mathbf{z},\theta,\phi) = \begin{bmatrix} \langle |E_v|^2 \rangle \\ \langle |E_h|^2 \rangle \\ 2\,\mathrm{Re}\langle E_v E_h^* \rangle \\ 2\,\mathrm{Im}\langle E_v E_h^* \rangle \end{bmatrix} \qquad (7)$$

In Equation (7), E_v and E_h are the vertically- and horizontally-polarized components of the field. The first two components of the Stokes-parameter vector represent average quantities, and carry information about the amplitude of the field. The other two components carry information about the phase [14]. The quantity $\bar{\bar{\mathbf{P}}}(\theta,\phi;\theta',\phi')$, in Equation (6), is a 4×4 phase matrix which describes the scattering properties from direction (θ',ϕ') into direction (θ,ϕ). The phase matrix is the sum of the Müeller matrices of all scatterers, per unit volume, at z. The explicit expressions of the phase-matrix elements, in terms of the scattering-amplitude tensor (Equations 2-5) have been reported in [15, 20]. $\bar{\bar{\kappa}}(\theta,\phi)$ is the extinction-coefficient matrix. It reflects the rate of intensity dissipation, due to scattering and ohmic losses, per unit volume. Its explicit expression, in terms of the scattering-amplitude tensor elements, can be found in [20].

Since both forest and vegetation are considered to be sparse media, having small albedo, the radiative-transfer equation has been solved, using an iterative approach, up to the second order with respect to the albedo [1, 21]. The explicit formulations of the zero-, first-, and second-order of the radiative-transfer equation are given in [1, 21], but will be summarized here for the sake of completeness.

2.4.1.1. Zero–order solution

The zero–order solution is considered to be the scattering from the ground, attenuated by vegetation. Its contribution to the total bistatic-scattering coefficient is given by

$$\sigma^0_{pq} = \left[\prod_{n=1}^{2} L_{np}(\theta_s) L_{nq}(\theta_i)\right] \sigma^s_{pq}(\theta_s,\phi_s;\pi-\theta_i,\phi_i) \qquad (8)$$

Here, $\sigma^s_{pq}(\theta_s,\phi_s;\pi-\theta_i,\phi_i)$ is the pqth element of the surface bistatic-scattering coefficient, where p is the polarization of the scattered signal, and q is the polarization of the incident signal. $L_{np}(\theta_s)$ is the propagation loss in either the crown (n=1) or the trunk (n=2), with

$$L_{np}(\theta) = \exp\left[-k_{np}(\theta) H_n \sec\theta\right] \qquad (9)$$

where $k_{np}(\theta)$ is the ppth element of the extinction matrix reported in (6), and H_n is the nth layer depth. The subscripts i and n represent incident and scattered directions, respectively.

2.4.1.2. First-order solution

The first-order solution is given by

$$\sigma^1_{pq} = \sigma_{pq}(C) + \sigma_{pq}(C \leftrightarrow g) + \sigma_{pq}(T) + \sigma_{pq}(T \leftrightarrow g) \qquad (10)$$

In Equation (10), the first term stands for crown scattering, the second term stands for the crown-ground interaction, the third term stands for the trunk scattering and the last term stands for the trunk-ground interaction.

The crown scattering term:

$$\sigma_{pq}(C) = Q_{1pq}(\theta_s,\phi_s,\pi-\theta_i,\phi_i)\left[\frac{1-L_{1p}(\theta_s)L_{1q}(\theta_i)}{k_{1p}(\theta_s)\sec\theta_s + k_{1q}(\theta_i)\sec\theta_i}\right] \qquad (11)$$

where $Q_{1pq}(\theta_s,\phi_s,\pi-\theta_i,\phi_i)$ is the pqth element of the matrix, $\bar{\bar{\mathbf{P}}}(\theta_s,\phi_s,\pi-\theta_i,\phi_i)$, within the crown layer.

The crown-ground interaction term:

This term is the sum of two terms. The first term crown-ground interaction. It represents scattering from a stem, or leaf, followed by scattering from the ground. The term is the ground-crown interaction, and can be thought reverse path.

$$\sigma_{pq}(C \leftrightarrow g) = \sigma_{pq}(C \to g) + \sigma_{pq}(g \to C)$$

$$\sigma_{pq}(C \to g) = \int_0^{2\pi} d\phi_i \int_0^{\pi/2} \sin\theta_i \, d\theta_i \sum_{u=v,h} \left\{\left[\prod_{n=1}^{2} L_{np}(\theta_s) L_{nu}(\theta_i)\right] \sigma^s_{pu}(\theta_s,\phi_s,$$

$$\left[\frac{\cos\theta_i}{L_{nu}(\theta_i)} Q_{1uq}(\pi-\theta_i,\phi_i,\pi-\theta_i,\phi_i) \frac{L_{1u}(\theta_i)-L_{1q}(\theta}{k_{1q}(\theta_i)\cos\theta_i - k_{1u}(\theta}\right.$$

Using reciprocity, it is easy to show that

$$\sigma_{pq}(C \to g) = \sigma_{pq}(g \to C)$$

The trunk scattering term:

The formulation of trunk scattering can be obtained Equation (11) by replacing the subscript 1 with 2, and multiplying by the two-way propagation losses, S_{pq} within the crown with

$$S_{pq} = L_{1p}(\theta_s) L_{1q}(\theta_i)$$

The trunk-ground scattering term:

Similar to Equation (12), the trunk-ground scattering has terms: scattering from the trunk followed by scattering from ground, and scattering from the ground followed by scattering the trunk. The explicit expression for each term can be obtained from Equation (13), by replacing the subscript 1 with 2 and multiplying by the propagation losses through the crown layer, given Equation (15).

2.4.1.3. The second-order scattering

The second-order solution of the radiative-transfer equation contains many terms. They can be grouped in accordance with different scattering mechanisms. One includes those terms that result from a double bounce between two scatterers within the layer. The second includes those terms which result from a bounce, between a scatterer in the crown layer, and the trunk. The explicit expression of these terms is given in [1, 21]. It is worth noting that the second-order terms are computationally intensive. Furthermore, they may or may not contribute significantly to the total backscattering coefficient, depending on the size of the scatterer relative to a wavelength. Therefore, the reader is referred to [1, 21] for a detailed discussion.

2.4.2. Signal statistics for a forest canopy

An approach to find the signal distribution by numerical simulation has been developed, to provide information on the

nal-amplitude distribution of forest components, modeled as needles, disks, or finite-length dielectric cylinders. The simulation involves:

(1) Establishing three-dimensional grids within a volume of a five-wavelength cube;

(2) discretizing the orientation of each forest component into $N \times M$ possible orientations in the azimuth and zenith directions [22];

(3) locating a forest component with a randomly-selected orientation at each grid point;

(4) computing the scattered field from each forest component in the direction of the radar receiver; and

(5) summing up the total scattered field from each forest component, with an appropriate amount of attenuation by the forest canopy, to obtain a total scattered field sample at the radar receiver.

This procedure is repeated until a sufficiently-large number of samples (generally, around 2000) is obtained. From these samples, a distribution function can be estimated. Figure 3 is an example of the signal distributions obtained from using such a simulation technique. The figure gives the distribution functions for needle-shaped and disk-shaped leaves. In parts (a) and (b), where small leaf sizes are selected, the signal amplitudes follow the Rayleigh distribution, as expected. In part (c), larger disk-shaped leaves are selected for computation, and the distribution function becomes Gamma distributed. Such a change in distribution has not been reported from experimental investigations in the past, because a well-defined signal distribution curve requires a very large number of samples, not usually available from experimental studies.

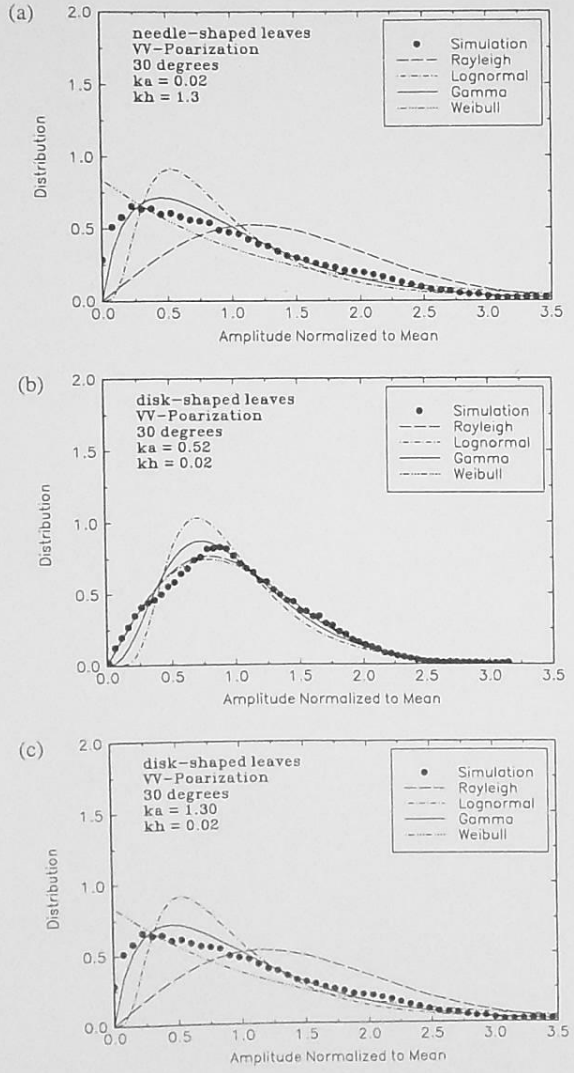

Figure 3. Signal distribution from tree leaves with nearly-horizontal orientation: (a) needle-like leaves, (b) small disk-like leaves , and (c) large disk-like leaves. [24]

3. Verifying the model against measurements

Verification of the model is carried out first on the component level, and then the complete model is tested against measured data. In the following subsections, each case will be considered.

3.1. Verifying the component models against measurements

The predicted values of the backscattering cross section and the extinction efficiencies from some forest components, are compared with controlled laboratory measurements, and shown in Figures 4-6. Figure 4 gives a comparison between the calculated and measured values of the extinction efficiency, associated with branches modeled as finite cylinders [25]. Figure 5 depicts a comparison between the calculated and measured values of the backscattering cross section, for a circularly-polarized plane wave exciting circular discs, used to model coniferous leaves [18]. Three different sizes are illustrated. Figure 6 depicts a comparison between the calculated and measured values of the backscattering cross section, for a circularly-polarized plane wave exciting dielectric rods with different radii, which can be used to model coniferous leaves or stems [18].

In Figure 7, the validity of the irregular-soil-surface model has been verified, through comparison with laboratory-controlled measurements from a Gaussian-height and Gaussian-correlated

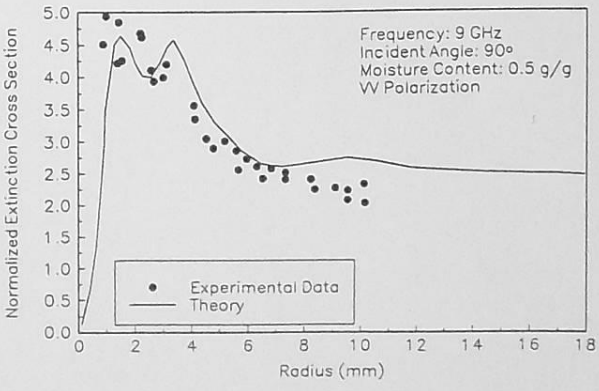

Figure 4. Comparison between the measured and calculated values of the extinction efficiency for branches, as a function of the branch radius [25].

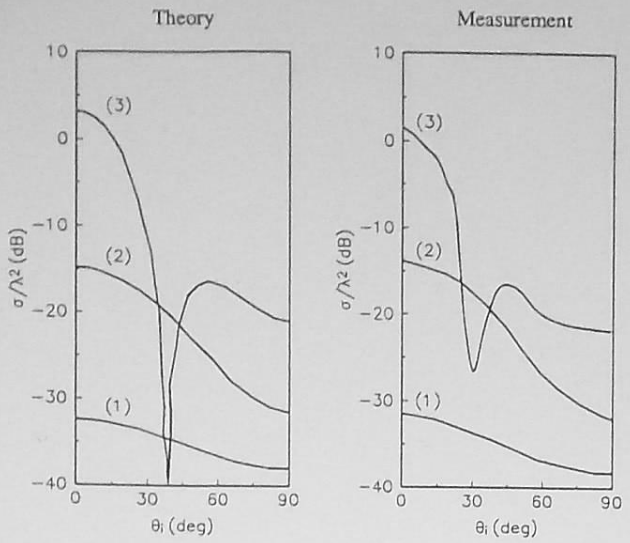

Sample Number	(1)	(2)	(3)
ka	0.7620	1.5230	3.0420
h/a	0.1060	0.1000	0.1009
$Re(\varepsilon_r)$	3.1200	3.1100	3.1000

Figure 5. Comparisons between the calculated and measured backscattering cross sections of a circularly-polarized plane wave exciting circular disks [18].

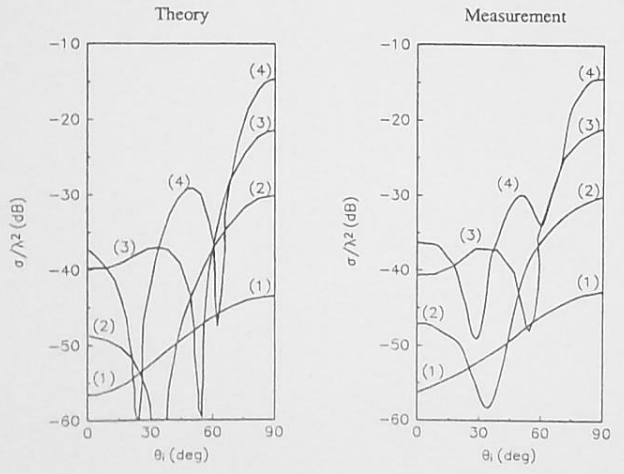

Sample Number	(1)	(2)	(3)	(4)
ka	0.1143	0.1904	0.26666	0.3428
h/a	10.0000	9.9900	9.9900	10.0000
$Re(\varepsilon_r)$	3.1300	3.1300	3.1500	3.1400

Figure 6. Comparisons between the calculated and measured backscattering cross sections of a circularly-polarized plane wave exciting dielectric rods [18].

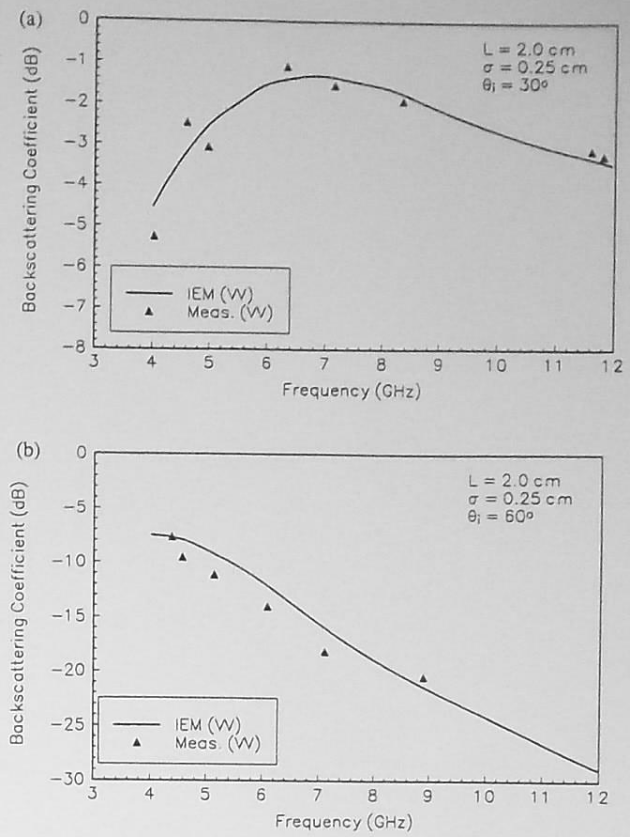

Figure 7. Comparison of the rough-surface scattering-model predictions with laboratory-controlled measurements from a Gaussian height, Gaussian-correlated, perfectly-conducting surface with an rms height of 0.25 cm, and a correlation length of 2 cm. (a) 30° incidence angle, (b) 60° incidence angle. [19]

perfectly-conducting surface [19]. The surface roughness is represented by a Gaussian correlation function, with correlation length L, and standard deviation σ [10, 20].

3.2. Verifying the forest-canopy model against measurements

Comparisons of the forest-scattering model with measurements are shown in Figures 8-11. In Figures 8 and 9, comparisons are made between calculated and measured values for the backscattering coefficients from a walnut canopy, at two different frequency bands [1]. In Figures 10 and 11, the forest model is compared with backscattering measurements from Nordmann Spruce and Norway Spruce [25]. In all figures, good agreement is found between the measured and predicated values of the backscattering coefficient.

4. Examples of model application

One application of the scattering model is to understand how the forest-scattering characteristics are related to the canopy parameters. To achieve this goal, three examples are considered.

Example 1:

The relationship between the tree architecture and the radar signal is investigated at X-band through experimental studies [25].

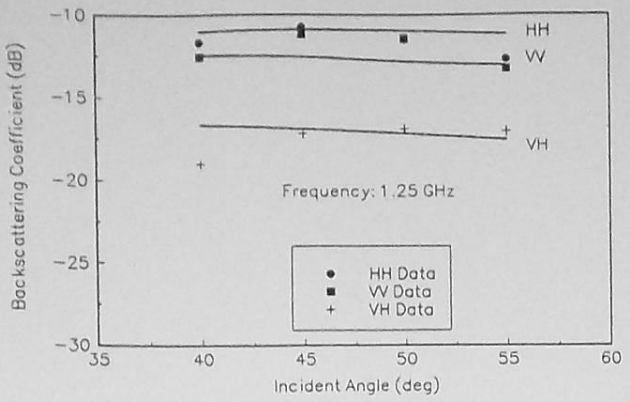

Figure 8. Comparisons of theoretical and experimental backscattering coefficients for a walnut canopy at L-band (1.25 GHz), as a function of the incidence angle [1].

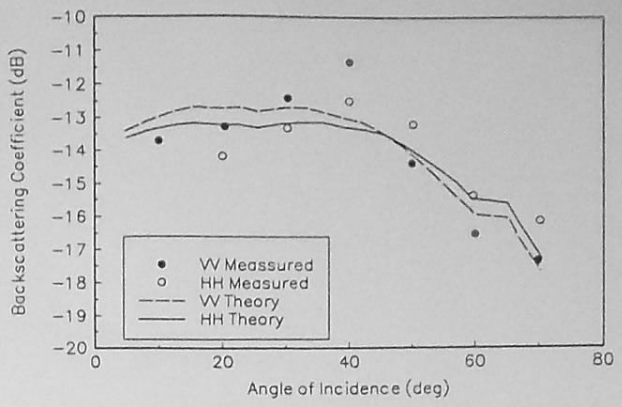

Figure 11. Comparisons of theoretical and experimental backscattering coefficients for a Norway spruce tree at X-band (10 GHz), as a function of the incidence angle [25].

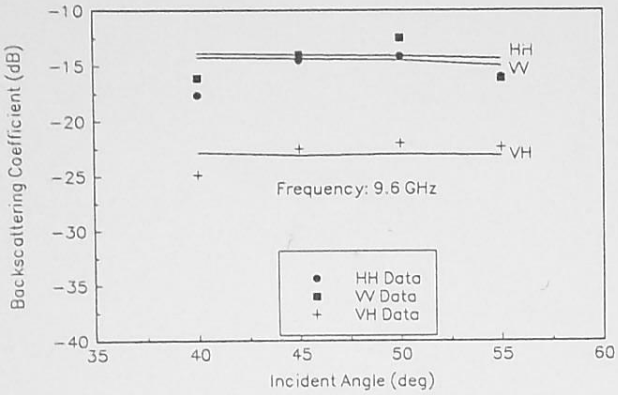

Figure 9. Comparisons of theoretical and experimental backscattering coefficients for a walnut canopy at X-band (9.6 GHz), as a function of the incidence angle [1].

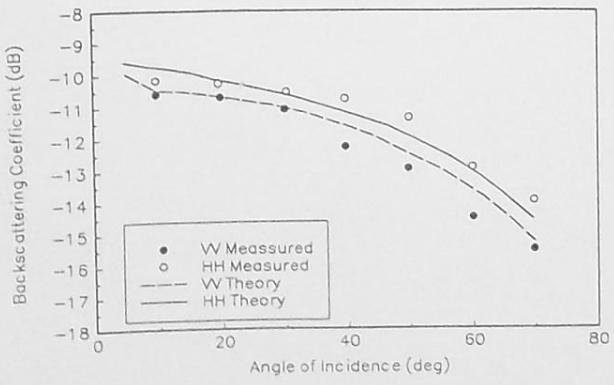

Figure 10. Comparisons of theoretical and experimental backscattering coefficients for Nordmann spruce tree at X-band (10 GHz), as a function of the incidence angle [25].

The interpretation of these experimental results is carried out with the help of the scattering model. According to the forest-scattering model, the major scattering trend at X-band is due to the leaves, while the perturbation to the angular trend, and the level difference between the vertically- and horizontally-polarized backscattering coefficients, are due to the branch-orientation distributions.

Example 2:

An application of the scattering model to walnut trees [1] leads to the following conclusions:

(i) To obtain a match between the calculated and measured values of the backscattering coefficients, the branch-size distribution is important.

(ii) Small branches and leaves generally contribute to the backscattering coefficients at X-band.

(iii) The contribution of the trunk-soil interaction to the backscattering coefficients depends heavily on soil moisture, and is more important for horizontally-polarized waves than vertically-polarized waves.

Example 3:

A numerical-simulation study of the radar return from a canopy, modeled as a half space containing only one kind of forest components (leaves or branches) [24], reveals the following power-distribution function properties:

(i) The power returned from a half-space of needle-shaped leaves follows the Rayleigh distribution when the needles are short, and resembles the Gamma distribution when the needles are long.

(ii) The distributions of power returned from disk-shaped leaves depend on the leaf orientation. For horizontally-oriented leaves, the power return statistics follow the Weibull distribution. For vertically-oriented leaves, the Gamma distribution gives the best fit to the power distribution.

5. Conclusions

The WSRC at UTA is committed to the development of completely-realistic models, such as the IEM surface model and the forest-canopy model, useful for use throughout the world among the remote-sensing communities. Our current canopy model is superior to many existing models, because it accounts for second-order volume scattering, it uses a rough-surface model to account for the canopy-ground interactions, it is applicable over frequencies ranging from P-band to X-band, and it is fully polarimetric.

The application of the model to several forest-canopy types leads to a quantitative understanding of the relationships between the forest parameters and the backscattering coefficients. These relationships are of great help in determining the optimum radar parameters (i.e., frequency, polarization, and incident angle) for extracting certain forest parameters of interest (i.e., soil moisture, biomass, leaf-area index), and to correct for the effect of other parameters.

Future applications will make use of the model in estimating signal interference in radio-wave communication, due to scattering from earth terrain. There are also plans to connect the model with ecosystem dynamic models, for environmental and global-change studies. The ecosystem dynamic models address the issue of successive changes in the forest composition and structure [26].

Acknowledgment

This work was supported by NASA under Grant NAGW-3091.

References

1. M. A. Karam, A. K. Fung, R. H. Lang, and N. S. Chuahan, "A microwave scattering model for layered vegetation," *IEEE Trans. Geosci. Rem. Sens.*, **GRS-30**, No. 4, pp. 767-784, 1992.

2. J. A. Richards, G.-Q. Sun, and D. S. Simonett, "L-band radar backscatter modeling of forest stands," *IEEE Trans. Geosci. Rem. Sens.*, **GRS-23**, No. 4, pp. 487-498, 1987.

3. S. L. Durden, J. J. Van Zyl, and H. A. Zebker, "Modeling and observation of radar polarization signature of forested areas," *IEEE Trans. Geosci. Rem. Sens.*, **GRS-27**, No. 3, pp. 290-301, 1989.

4. F. T. Ulaby, K. Sarabandi, K. McDonald, M. Whitt, and M. C. Dobson, "Michigan microwave canopy scattering model," *Int. J. Rem. Sens.*, **11**, No. 7, pp. 1223-1253, 1990.

5. K. C. McDonald, M. C. Dobson, and F. T. Ulaby, "Using MIMICS to model L-Band multiangle and multitemporal backscatter from a walnut orchard," *IEEE Trans. Geosci. Rem. Sens.*, **GRS-28**, No. 4, pp. 477-491, 1990.

6. K. C. McDonald, M. C. Dobson, and F. T. Ulaby, "Modeling multi-frequency diurnal backscatter from a walnut orchard," *IEEE Trans. Geosci. Rem. Sens.*, **GRS-29**, No. 6, pp. 852-863, 1991.

7. M. A. Karam, and A. K. Fung, "Leaf-shape effects in electromagnetic wave scattering from vegetation," *IEEE Trans. Geosci. Rem. Sens.*, **GRS-27**, No. 6, pp. 687-697, 1989.

8. M. A. Karam and A. K. Fung, "Electromagnetic scattering from a layer of finite randomly oriented, dielectric, circular cylinders over a rough interface with application to vegetation," *Int. J. Rem. Sens.*, **9**, No. 6, pp. 1109-1134, 1988.

9. M. A. Karam and A. K. Fung, "Scattering from randomly oriented circular discs with application to vegetation," *Radio Science*, **18**, pp. 557-563, 1983.

10. M. A. Karam and A. K. Fung, "Scattering from randomly oriented scatterer of arbitrary shape in the low frequency limit with application to vegetation, *Digest of International Geoscience and Remote Sensing Symposium (IGARSS'83)*, pp. 2.5.1-5.7, 1983.

11. N. S. Chauhan, R. H. Lang, and K. J. Ranson, "Radar modeling of a boreal forest," *IEEE Trans. Geosci. Rem. Sens.*, **GRS-29**, No. 4, pp. 627-638, 1991.

12. A. K. Fung and H. S. Fung, "Application of first order renormalization method to scattering from a vegetation-like half space, *IEEE Trans. Geosci. Rem. Sens.*, **GRS-15**, pp. 189-195, 1977.

13. M. A. Karam, and A. K. Fung, "Vector forward scattering theorem," *Radio Science*, **17**, No. 4, pp. 752-756, 1982.

14. A. Ishimaru, *Wave Propagation and Scattering in Random Media*, New York, Academic Press, 1978.

15. L. Tsang, J. A. Kong, and R. T. Shin, *Theory of Microwave Remote Sensing*, New York, John Wiley & Sons, pp. 139-140, 1985.

16. F. T. Ulaby, and M. A. El-Rayes, "Microwave dielectric spectrum of vegetation, part II: Dual dispersion model," *IEEE Trans. Geosci. Rem. Sens.*, **GRS-25**, No. 5, pp. 550-557, 1987.

17. M. T. Hallikaninen, F. T. Ulaby, M. C. Dobson, M. A. El-Rayes, and L. Wu, "Microwave dielectric behavior of wet soil, part I: Empirical models and experimental observations," *IEEE Trans. Geosci. Rem. Sens.*, **GRS-23**, No. 1, pp. 25-34, 1985.

18. M. A. Karam, A. K. Fung, and Y. M. M. Antar, "Electromagnetic wave scattering from some vegetation samples," *IEEE Trans. Geosci. Rem. Sens.*, **GRS-26**, No. 6 , pp. 799-808, 1988.

19. A. K. Fung, Z. Li, and K. S. Chen, "Backscattering from a randomly rough dielectric surface," *IEEE Trans. Geosci. Rem. Sens.*, **GRS-30**, No. 6, pp. 799- 1992.

20. F. T. Ulaby, R. K. Moore, and A. K. Fung, *Microwave Remote Sensing: Active and Passive, Vol. III*, Dedham, Artech House, 1986.

21. M. A. Karam, F. Amar, A. K. Fung, E. Mougin, A. Lopes, "Polarimetric signatures of coniferous forest canopy based on vector radiative transfer theory," submitted to *Remote Sensing of Environment*, November, 1992.

22. J. A. Kong, A. A. Swartz, H. A. Yueh, L. M. Novak, and R. T. Shin, "Identification of terrain cover using the optimum polarimetric classifier," *J. Electromag. Waves Applica.*, **2**, No. 2, pp. 171-194, 1987.

23. F. T. Ulaby, K. Sarabandi, and A. Nashashibi, "Statistical properties of the Müeller matrix of distributed targets," *IEE Proc. (F)*, **139**, No. 2, pp. 136-146, 1992.

24. M. A. Karam, K. S. Chen and A. K. Fung, "Statistics of backscatter radar return from vegetation," *Digest International Geoscience and Remote Sensing Symposium (IGARSS'92)*, pp. 242-244, 1992.

25. E. Mougin, A. Lopes , M. A. Karam, and A. K. Fung, "Effect of tree structure on X-band microwave signature of coniferous," *IEEE Trans. Geosci. Rem. Sens.*, to be published in 1993.

26. P. J. Sellers, F. G. Hall, D. E. Strkel, G. Asrar, and R. E. Murphy, "Satellite remote sensing and field experiments," in R. J. Hobbs and H. A. Mooney (eds.), *Remote Sensing of Biosphere Functioning*, New York, Springer-Verlag, 1989.

Introducing Feature Article Authors

Mostafa A. Karam received the BSc degree (with first honor) and the MSc degree, both in electrical engineering, from Cairo University, Giza, Egypt, in 1977 and 1980, respectively. He received the PhD degree in electrical engineering from the University of Kansas, Lawrence, Kansas in 1984.

During the period 1977-1980, he worked as a teaching assistant at Cairo University. He was with the Remote Sensing Laboratory, at the University of Kansas, as an Assistant Project Engineer, from 1980-1984. He has been with the Wave Scattering Research Center, at the University of Texas at Arlington, as a Faculty Associate, since 1984. He has contributed to and served as a reviewer for several technical journals in the areas of applied physics, applied electromagnetics, waves in random media, and microwave remote sensing. His recent research interests include forest polarimetric signatures, interference in radio-wave communication systems due to scattering from earth terrain, and land surface-atmosphere interaction, and its roles in global change.

Dr. Karam is a co-Founder and the present Chairman of the IEEE Antennas and Propagation Society's Fort Worth Chapter. He is a member of the Electromagnetics Academy, and is listed in *Who's Who in Electromagnetics in 1990*.

Faouzi Amar received a DEUS degree in mathematics and physics from the University Mohammed V, in Rabat, Morocco, in 1980, and a BSEE (with honors) and an MSEE, from the University of Texas at Arlington, in 1986 and 1989, respectively. He is currently working toward a PhD in Electrical Engineering at the WSRC.

From 1989 to 1991, Mr. Faouzi Amar worked as project manager and design engineer at the Electromechanics Company, where he designed several antennas for use in EMC and EMI testing. He rejoined UTA under a NASA fellowship. Currently, he is a Graduate Research Assistant and an instructor at UTA. He has also written a book on numerical methods.

Mr. Faouzi Amar served as Secretary to the Fort Worth AP-S Chapter during 1992. He is also a member of the Applied Computational Electromagnetics Society and HKN.

Adrian K. Fung received the BS degree from Cheng Kung University, Taiwan, China, in 1958, the MSEE degree from Brown University, Providence, Rhode Island, in 1961, and the PhD degree from the University of Kansas, Lawrence, in 1965.

From 1965 to 1984, he was on the faculty of the Department of Electrical Engineering, University of Kansas. In the fall of 1984, he joined the University of Texas at Arlington, where he is now a Professor with the Electrical Engineering Department, and Director of the Wave Scattering Center. His research interests have been in the areas of radar-wave scattering and emission from earth terrains and sea, and radar and ISAR image generation, simulation, and interpretation. He has contributed to many book chapters, and is a co-author of the three-volume book, *Microwave Remote Sensing* (Artech House: vol. 1, 1981; vol. 2, 1982; vol. 3, 1986).

Dr. Fung has served as an Associate Editor of *Radio Science* and IEEE JOE. He was the recipient of the Halliburton Excellence in Research Award in 1986, the Distinguished Research Award of the University of Texas at Arlington, and the 1989 Distinguished Achievement Award from the IEEE Geoscience and Remote Sensing Society.

Mostafa A. Karam

Faouzi Amar

Adrian K. Fung